# Instruments and methods for measuring the backward-scattering coefficient of ocean waters

Robert A. Maffione and David R. Dana

The backward-scattering coefficient $b_b$ is an important optical property that plays a central role in studies of ocean-color remote sensing, suspended particle distributions, water clarity, and underwater visibility. We investigate the fixed-angle backscattering sensor approach for the application of measuring $b_b$. Analysis shows that the sensor response to volume scattering can be expressed as the integral of the volume scattering function (VSF) over the backward angles (90–180°) weighted by the sensor-response function. We present a procedure for determining the sensor-response function that contains all the information necessary to calibrate the sensor fully to measure the VSF at a nominal backscattering angle. It is shown that, for fixed-angle backscattering sensors, $b_b$ is most accurately estimated when the sensor-response function covers the middle range of backscattering angles, roughly 110–160°, where the shape of the VSF has the least variability. Backscattering at and near the end angles, namely, 90° and 180°, are least correlated with $b_b$. We describe a variety of spectral backscattering sensors that we have developed, and we present their sensor-response functions. 

*Key words:* Ocean optics, backscattering, oceanographic instruments.

## 1. Introduction

The backward-scattering coefficient $b_b$ is of fundamental importance to ocean-color remote sensing. Although spectral absorption by ocean water modifies the spectrum of the submarine light field, it is spectral backscattering, predominantly by suspended particles, that provides the remotely sensed optical signal. The measured intensity of the light backscattered by the ocean, which is used to infer the concentration of ocean water constituents such as phytoplankton, is of limited value without knowledge of $b_b$. Historically a great deal of attention has been devoted to developing instruments and methods for determining spectral absorption of ocean water and its individual constituents. (See Pegau *et al.*[1] for a review of the many methods available for measuring absorption.) Ironically, however, there has been a surprising lack of attention to directly measuring the backward-scattering coefficient, particularly spectrally.

Here we describe instruments and methods for directly measuring backward light scattering by ocean water in calibrated units of the volume scattering function (VSF) (per meter per steradian) or the backward-scattering coefficient (per meter). These instruments and methods were initially developed over many years at SRI International, and these experiments are now continuing at Hydro-Optics, Biology, and Instrumentation Laboratories. A unique calibration method, presented in detail here, is used to convert the optical backscattering signal to a measurement of the VSF at a nominal backscattering angle. The particular angle depends on the optical geometry of the instrument and, to a much lesser degree, the shape of the VSF in the backward hemisphere as well as the attenuation coefficient of the water. Multiplying this measured VSF by a suitable conversion factor then converts the VSF to $b_b$. The shape of the VSF in the backward hemisphere, generally known from measurements by others (e.g., Petzold[2] and Kullenberg[3]) and from calculations with Mie theory, greatly constrains the values of the conversion factor so that use of a constant value results in a likely standard error in $b_b$ of ~10%. A previously published analysis by Oishi[4] shows that the maximum likely error is ~17% of the estimated value of $b_b$ by this method. Regardless of any error in the conversion to $b_b$, measurement of the VSF at a nominal backward angle is shown to be highly accurate and is partially traceable to a National Institute of

During part of this study R. A. Maffione was with the College of Oceanic and Atmospheric Sciences, Oregon State University, Corvallis, Oregon 97333. Both authors are now with Hydro-Optics, Biology, and Instrumentation Laboratories, Moss Landing, California 95039.

Received 20 June 1996; revised manuscript received 1 May 1997.
0003-6935/97/246057-11$10.00/0

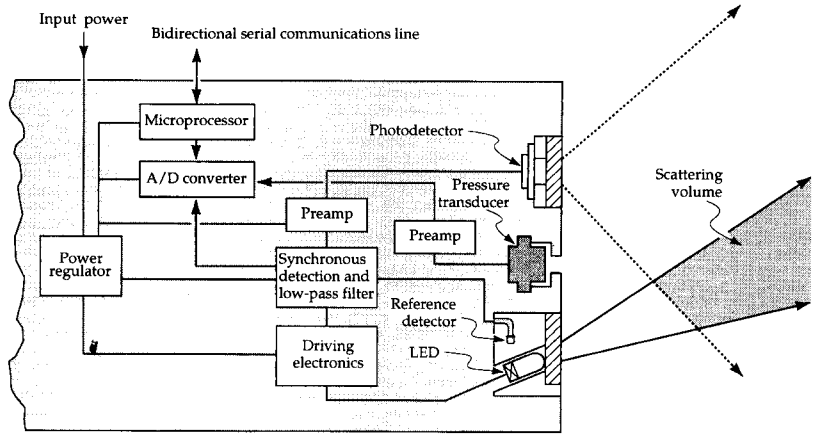


Fig. 1. Schematic layout of the backscattering sensor developed at SRI International in the early 1980's under an Advanced Research Projects Agency program called LIDEX.

Standards and Technology standard. It is therefore recommended that the calibration method presented here be adopted as a standard protocol for measuring the VSF in the backward hemisphere, which should greatly aid in the comparison and interpretation of worldwide measurements.

## 2. Background

### A. History

Højerslev[5] credits Pettersson[6] with constructing the first *in situ* optical backscattering sensor. Pettersson's instrument used an incandescent light bulb and two large-area photocells. The sensor did not incorporate spectral filters and was not calibrated to provide measurements in units of an optical property, such as the VSF at a nominal angle or $b_b$. However, given the technology of the time, Pettersson's instrument was impressive and marks a milestone in the development of ocean-optical backscattering sensors.

General-angle scattering meters, sometimes referred to as nephelometers, started to be developed in the late 1950's and early 1960's for *in situ* studies. To our knowledge, the first published paper on a submersible, general-angle scattering meter was by Tyler and Richardson[7] in 1958. Their instrument covered the angular range from 20° to 170° and was calibrated to give measurements in units of the VSF (per meter per Steradian). In theory a properly calibrated general-angle scattering meter provides the most accurate way of determining $b_b$, since it measures the VSF over a range of backscattering angles. However, this type of instrument is notoriously difficult to calibrate accurately, and it is cumbersome and time-consuming to deploy. Kullenberg[3] gives a review of the various submersible general-angle scattering meters until that time and discusses some of the problems with their calibrations. The current study is concerned with fixed-angle optical backscattering sensors and their calibration for spectrally determining the VSF at a nominal backscattering angle as well as the backward-scattering coefficient.

The first fixed-angle backscattering sensors designed and calibrated for measuring the VSF of ocean water were developed at SRI International[8] in the early 1980's under a program funded by the Advanced Research Projects Agency. The program was called LIDEX for light detection experiment. These sensors used infrared light-emitting diodes (LED's) and high-frequency phase-synchronous photodetection. The major advantages in using an LED as the light source are its relatively low power consumption and ability to be modulated electronically at rapid rates. The drawback at that time was that the only available LED's that were bright enough for the application of measuring backscattering by ocean water were IR LED's. The original SRI backscattering sensors used visible-blocking filters and measured backscattering over the spectral bandwidth of the LED centered at 880 nm. Figure 1 shows a schematic layout of this sensor.

The absolute calibration was based on the sensor's response to a reflectance standard. This method involved measuring the response of the sensor to a Lambertian target as a function of range from the sensor. The resulting calibrated measurement provided an estimate of the VSF (per meter per steradian) at a nominal backscattering angle.[8] Later a more rigorous analysis by Maffione *et al.*[9] of this calibration scheme showed that, for the original sensor geometry, the backscattering angle was nominally 150°. The analysis by Maffione *et al.* improved the accuracy of the calibration by taking into account geometrical factors that had previously been neglected.

It is possible to use other types of light source at the expense of some of the advantages of LED's. In the late 1980's members of the Johns Hopkins University Applied Physics Laboratory developed a backscattering sensor using a bright incandescent lamp (Smart *et al.*[10]). These sensors incorporated spectral absorption filters centered at 490 and 532 nm., giving the sensors the distinction of being the first visible-wavelength, fixed-angle backscattering sensors. The optical geometry was designed to yield a mea-

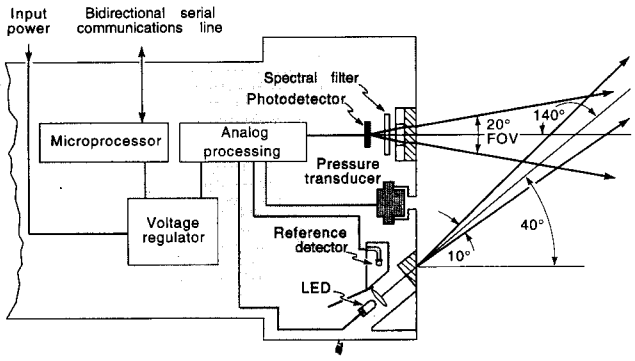


Fig. 2. Second-generation backscattering sensor developed at SRI in 1991. The major improvement was better collimating optics for application in the visible spectrum (400 to 700 nm) and for estimating $b_b$.

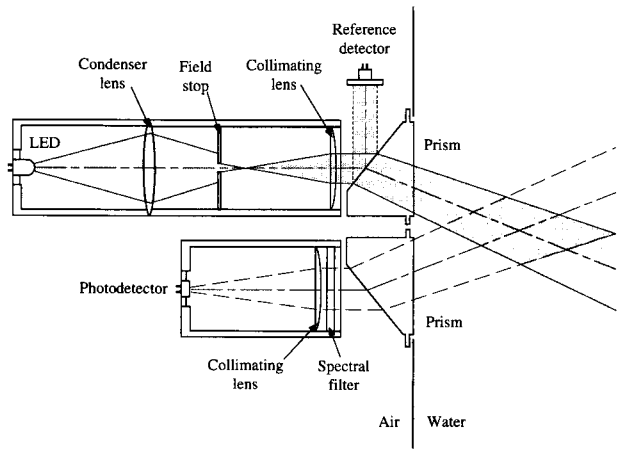


Fig. 3. Optical layout of the BB-4, BBC-4, and HydroScat-6. The HydroScat-6 does not include the condenser lens but instead uses a single, fast achromat.

surement of the VSF at a centroid angle of 170°, which is desirable for lidar applications (although 170° is undesirable for estimating the backward-scattering coefficient).

The next advance came in 1991 when we redesigned the optics and electronics of the SRI's IR sensor to take advantage of visible-wavelength LED's. Figure 2 shows a schematic of this sensor, illustrating its more narrow optical geometry that resulted in a measurement of the VSF at a nominal angle of 135°. The lower backscattering angle was necessary to estimate $b_b$ more accurately from a single-angle VSF measurement (explained below). We first deployed the newly modified sensors during the Office of Naval Research ocean-optical closure experiment at Lake Pend Oreille, Idaho, in the spring of 1992. We used only one visible wavelength, centered at 565 nm, in the newly modified sensors because sufficiently bright LED's were not yet available at other visible wavelengths. When bright LED's at a variety of visible wavelengths later became available, we developed a five-wavelength backscattering sensor[11] that was incorporated into a remotely operated vehicle.[12] This multiwavelength sensor, dubbed the Slab, incorporated the same optical and electrical design as the single-wavelength visible sensor.

Following this achievement we completely redesigned both the optics and electronics so that a more compact and robust multiwavelength backscattering sensor could be developed. The first version was a four-wavelength backscattering sensor called the BB-4. A second version included a four-wavelength, folded-path beam transmissometer and was called the BBC-4. The final version, which is now available commercially, is a six-wavelength backscattering sensor called the HydroScat-6. The optical layout of these sensors is shown in Fig. 3. These new sensors incorporate a unique electro-optical scheme that effectively cancels any ambient light signal. Thus maximum signal gain can be used even near the surface in bright sunlight. Narrow-band interference filters appropriately chosen within the broader spectral bands of the LED's are used in the receiving optics to select the measurement wavelengths. Each spectral channel has its own unique modulation frequency so that the receivers detect only the backscattered LED light from their respective channels. Thus a 670-nm receiver, for example, does not detect fluorescence excited by an adjacent, shorter-wavelength LED. Conversely, the receiver's modulation frequency can be dynamically phase locked to another channel so that it can detect fluorescence if this is desired.

### B. Notation and Definitions

The angular distribution of scattering by a small volume can be described by the VSF $\beta(\psi)$, defined as the second partial derivative of the scattered flux $\Phi$ with respect to solid angle $\Omega$ and scattering volume $V$, normalized by the incident, collimated irradiance $E$, viz.,

$$\beta(\psi) = \partial^2\Phi(\psi)/E\partial\Omega\partial V, \tag{1}$$

where $\psi$ is the polar scattering angle with respect to the collimation axis of the incident irradiance. Although not shown explicitly, $\beta(\psi)$ is a function of wavelength $\lambda$. In the ocean $\beta(\psi)$ also varies with time and space but is usually denoted as a function of only depth $z$.

Two useful optical properties can be derived from $\beta(\psi)$: the total scattering coefficient $b$ and the backward-scattering coefficient $b_b$. They are respectively defined by

$$b = \int_4 \int_\pi \beta(\psi)\mathrm{d}\Omega$$

$$= 2\pi \int_0^\pi \beta(\psi) \sin\psi \mathrm{d}\psi, \tag{2}$$

$$b_b = 2\pi \int_{\pi/2}^\pi \beta(\psi) \sin\psi \mathrm{d}\psi. \tag{3}$$

This latter optical property, $b_b$, finds its widest application in ocean-color remote sensing because it can be related in a simple though approximate way to the amount of solar light that is backscattered by the ocean, which in turn provides the spectrum of light emerging from the sea. For example, using the approximate two-flow (Shuster's) method or the method of successive scattering order starting with the full radiative transfer equation, one can show that, to first order, the irradiance reflectance is approximately $fb_b/a$, where $a$ is the absorption coefficient and $f$ is a factor that depends on certain environmental conditions.[13,14]

### 3. Theoretical Development and Calibration Methodology

The theoretical development and methodology presented here for calibrating an optical backscattering sensor and understanding its optical response and accuracy are completely general except for two constraints: the faceplate of the sensor is assumed to be flat and the optical geometry is fixed (in other words, it is a fixed-angle sensor). Note here that the term backscattering implies that the sensor measures light scattered through angles greater than 90°, i.e., the backward hemisphere. It is of course possible to construct a backscattering sensor with a faceplate that is not flat; for example, it could be concave, such as in the design of some free-angle nephelometers (see, for example, the description by Jerlov[15]), or it could be a right-angle faceplate so that the source and receiver are perpendicular, as in most *in situ* fluorometers. The analysis presented here could be extended to include a variety of faceplate designs, although for the application of measuring $b_b$ a nonflat faceplate design is discouraged. Calibrating such sensors by the method described in this paper could be quite complicated or impossible. Moreover, a nonflat faceplate can increase the likelihood that light scattering by the faceplate itself will contaminate the water scattering signal. This is especially problematic for a right-angle design such as that used in submersible fluorometers. Unless there is a compelling need for a nonflat faceplate, it is strongly recommended that future backscattering sensor designs incorporate a flat faceplate to allow for accurate calibration.

Figure 4 shows a schematic of the general optical geometry for a backscattering sensor. The fixed geometrical parameters that define the optical design of the sensor are the following:

- $H$ is the distance between optical axes of the source and detector,
- $\theta_{0s}$ is the in-water (i.e., refracted) angle of the source optical axis,
- $\theta_{0d}$ is the in-water angle of the detector optical axis,
- $\alpha_s$ is the FWHM divergence angle of the source,
- $\alpha_d$ is the FWHM field of view (FOV) of the detector.

Distinct from the fixed parameters are the geometrical variables, defined by Fig. 4 as the following:

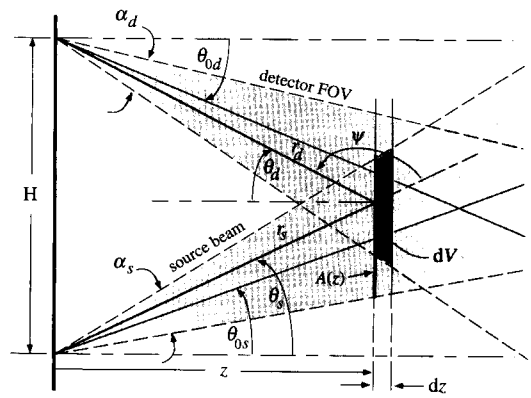


Fig. 4. Optical geometry for a generic fixed-angle backscattering sensor.

- $z$ is the linear distance perpendicular to the faceplate,
- $r_s$ is the water-path distance from the source to infinitesimal scattering volume,
- $r_d$ is the water-path distance from scattering volume to the detector,
- $\theta_s$ is the centerline angle of that portion of the source beam that illuminates scattering volume $dV$,
- $\theta_d$ is the centerline angle of that portion of the detector FOV that subtends intersecting scattering volume $dV$,
- $\psi$ is the scattering angle.

Note that the latter five variables can all be considered dependent variables of $z$. The dependent variable functions are all simple geometrical relationships involving fixed parameters.

In general the source beam has a finite area where it enters the water at the pressure window, which is not shown in Fig. 4. Likewise, the detector FOV has a finite area of acceptance at the water side of the window. These are omitted for simplicity and clarity in the presentation of the analysis but are easily taken into account by moving the origin of $z$, the axis perpendicular to the faceplate, further to the right in Fig. 4. Simple trigonometry can then be used to correct optical path lengths $r_s$ and $r_d$. If the areas are relatively small it is an excellent approximation to assume simply that the source and detector cones converge to a point at the window in the manner illustrated in Fig. 4.

Scattering volume $dV \equiv \Delta A dz/\cos\theta_s$ is defined by the intersection of the source beam and FOV of the detector, and it is a function of distance $z$. The intersecting volume is illustrated by the darker shaded region in Fig. 4. $\Delta A(z)$ is the area perpendicular to the $z$ axis subtended by $dV$ at the detector. Also note that path lengths $r_s$ and $r_d$ intersect at the center of $dV$ so that the angles that $r_s$ and $r_d$ make with the optical axis are likewise a function of $z$. At a certain distance denoted by, say, $z_{\text{mid}}$, lines $r_s$ and $r_d$ coincide with the source beam and detector optical axes, respectively. The scattering angle at $z_{\text{mid}}$, denoted

$\psi_{mid}$, is not, however, the scattering angle at the peak response of the sensor, nor is it the centroid scattering angle. This is made clear below.

Let $\Phi_0$ denote the radiant flux emitted into the water by the source beam. If $A(z)$ is the total area illuminated by the beam perpendicular to the $z$ axis, the flux $\Delta\Phi_{dV}(z)$ incident on d$V$ is

$$\Delta\Phi_{dV}(z) = \Phi_0 \exp(-cr_s)\Delta A(z)/A(z).$$

Irradiance $E$ incident on d$V$ is therefore

$$E(z) = \Delta\Phi_{dV}(z)/\Delta A(z)$$
$$= \Phi_0 \exp(-cr_s)/A(z).$$

By the definition of the VSF in Eq. (1), the flux scattered into the solid angle $\Delta\Omega$, which is determined by the FOV of the detector, is given by

$$\begin{aligned}\Delta\Phi(\psi, z) &= \beta(\psi)E(z)\Delta\Omega(z)\Delta V(z)\\ &= \beta(\psi)[\Phi_0 \exp(-cr_s)/A(z)][\Delta A(z) \cos\theta_d/r_d^2]\\ &\quad \times [\Delta A(z)dz/\cos\theta_s]\\ &= \beta(\psi)\Phi_0(\cos\theta_d/\cos\theta_s)[\exp(-cr_s)/r_d^2]\\ &\quad \times [\Delta A^2(z)/A(z)]dz, \end{aligned} \quad (4)$$

where infinitesimal dependent variables are replaced by their corresponding real, finite quantities. In the second line of Eq. (4) the last two bracketed quantities are $\Delta\Omega(z)$ and $\Delta V(z)$, as obtained from the geometry. The expression for $\Delta\Omega(z)$ assumes no vignetting at the detector, which is always true for the small optical path lengths involved with the types of backscattering sensors considered here. The scattered flux arriving at the detector's pressure window is then

$$\begin{aligned}\Delta\Phi_\beta(\psi, z) &= \Delta\Phi(\psi, z) \exp(-cr_d)\\ &= \beta(\psi)\Phi_0(\cos\theta_d/\cos\theta_s)\{\exp[-c(r_s + r_d)]/r_d^2\}\\ &\quad \times [\Delta A^2(z)/A(z)]dz\\ &= \beta(\psi)\Phi_0 W(z; c)dz, \end{aligned} \quad (5)$$

where

$$W(z; c) \equiv (\cos\theta_d/\cos\theta_s)\{\exp[-c(r_s + r_d)]/r_d^2\} \times [\Delta A^2(z)/A(z)] \quad (6)$$

is defined as the sensor-response weighting function to scattering. We denote the dependence of $W(z; c)$ on parameter $c$ explicitly to distinguish the weighting functions that result from waters with different attenuation coefficients. Note that $c$ is not the true beam attenuation coefficient but here represents the attenuation coefficient for the sensor's light-source beam. As shown below, $W(z; c)$ is a relatively weak function of $c$ so that even rough measurements or estimates of $c$ are adequate for an accurate attenuation correction.

Integration of Eq. (5) over all $z$ from 0 to $\infty$ gives the total flux scattered into $\Delta\Omega(z)$ arriving at the detector window. The response of the detector is proportional to this flux as well as to an electronic gain factor. For calibration purposes the detection electronics are usually designed to incorporate variable gain settings. Let the gain-factor setting for the detection of volume scattering be denoted $g_\beta$. This gain factor can be thought of as incorporating all electronic and optical conversion factors, such as detector efficiencies and losses, through the optical train. Then the detection signal denoted $\Phi_\beta$ is given by

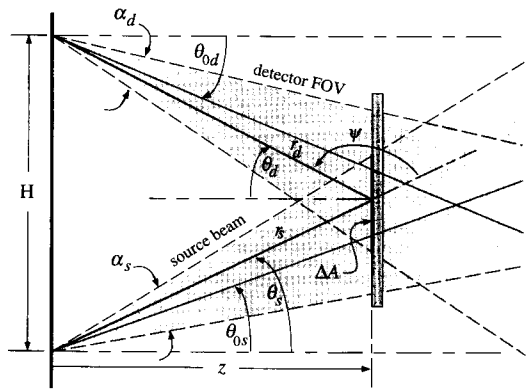


Fig. 5. Optical geometry for analyzing the sensor response to a Lambertian target.

$$\begin{aligned}\Phi_\beta &= \Phi_0 g_\beta \int_0^\infty \beta(\psi)W(z; c)dz\\ &= \Phi_0 g_\beta \beta(\psi^*) \int_0^\infty W(z; c)dz. \end{aligned} \quad (7)$$

The last step is justified by the integral mean value theorem; i.e., $\psi^*$ takes whatever value, within the limits of integration, that gives the equality in Eq. (7). As mentioned above, the scattering angle $\psi$ is implicitly a function of $z$. The value of $\psi^*$ depends both on $W(z; c)$ and the shape of the VSF. However, as shown below, $\psi^*$ is determined primarily by $W(z; c)$. The units of $\Phi_\beta$ are not relevant because the calibration described below involves a ratio of two measurements that cancels radiometric units. In other words, $g_\beta$ does not need to incorporate a quantum-electronic conversion factor to convert the electronic signal to absolute radiometric units such as watts.

The calibration method involves measuring the in-water response of the sensor to a Lambertian target as a function of $z$. Figure 5 illustrates the geometry with a Lambertian target at a distance $z$. The response of the sensor is similar to Eq. (6), but the VSF is replaced by a surface scattering function $\rho/\pi$, where $\rho$ is the diffuse reflectivity of the Lambertian target. Because the target is Lambertian, the surface scattering function is independent of scattering angle. Similarly to the derivation for the response of the sensor to volume scattering, the surface scatter-

ing response denoted $\Delta\Phi_\rho(z)$ to a Lambertian target at a distance $z$ is found to be

$$\Delta\Phi_\rho(z) = \Phi_0 g_\rho(\rho/\pi)\cos^2\theta_d\{\exp[-c_w(r_s + r_d)]/r_d^2\} \times [\Delta A^2(z)/A(z)] = \Phi_0 g_\rho(\rho/\pi)(\cos\theta_s \cos\theta_d)W(z; c_w). \quad (8)$$

In this case we denote the beam attenuation coefficient $c_w$ to distinguish it from $c$ in Eq. (7), which is the attenuation coefficient of the (e.g., ocean) water whose backscattering properties are being measured. $\Delta\Phi_\rho(z)$ is assumed to be measured in clear filtered water so that the target surface scattering greatly dominates the water volume scattering. The important difference between Eqs. (8) and (5) is the cosine factors. The $\cos\theta_s$ factor is missing in the denominator of Eq. (8) because there is no $dV \equiv \Delta A dz/\cos\theta_s$, since Eq. (8) deals with surface scattering. The additional $\cos\theta_d$ factor arises because the intensity of the scattered light from a plane Lambertian source varies as the cosine of the angle from the surface normal direction. It is important to distinguish this from the radiance emitted by a Lambertian source, which is constant with direction. Multiplying Eq. (8) by $dz/\cos\theta_s \cos\theta_d$ and integrating yields

$$\Phi_\rho = \int_0^\infty \frac{\Delta\Phi_\rho(z)}{\cos\theta_s \cos\theta_d} dz = \Phi_0 g_\rho(\rho/\pi)\int_0^\infty W(z; c_w)dz. \quad (9)$$

Taking the ratio of Eqs. (7) and (9) and solving for $\beta(\psi^*)$ gives

$$\beta(\psi^*) = \frac{\Phi_\beta}{g_\beta}\left(\frac{\rho}{\pi}\frac{g_\rho}{\Phi_\rho}\right)\frac{\int_0^\infty W(z; c_w)}{\int_0^\infty W(z; c)} = \frac{\Phi_\beta}{g_\beta}\mu\sigma(c, c_w), \quad (10)$$

where

$$\mu \equiv (\rho/\pi)(g_\rho/\Phi_\rho), \quad (11)$$

$$\sigma(c, c_w) \equiv \int_0^\infty W(z; c_w)\Big/\int_0^\infty W(z; c). \quad (12)$$

Thus one can convert the direct backscattering measurement $\Phi_\beta$ to $\beta(\psi^*)$ by normalizing $\Phi_\beta$ by the electronic gain factor $g_\beta$, which is set at the time of the measurement, and multiplying by the calibration constant $\mu$ and the attenuation correction factor $\sigma(c, c_w)$. Since Eq. (10) involves the ratio of the two gain factors $g_\beta$ and $g_\rho$, they need to be known only relative to each other. In other words, it is not necessary to know the various electronic and optical conversion factors implicitly incorporated into $g_\beta$ and $g_\rho$.

The constant calibration factor $\mu$ can be determined by measurement of the response of the sensor, usually in a laboratory tank containing filtered water, to a Lambertian target as a function of range $z$. This measurement yields $\Delta\Phi_\rho(z)$, as given by Eq. (8). Integration of $\Delta\Phi_\rho(z)/\cos\theta_s \cos\theta_d$ then gives $\Phi_\rho$, as in Eq. (9). The cosine factors $\cos\theta_s \cos\theta_d$ needed in the integration of $\Delta\Phi_\rho(z)$ are easily derived from the geometry in Fig. 5 and can be computed numerically. Spectralon is recommended as the Lambertian target because its reflectivity is known to high accuracy and does not change in water when its surface is properly wetted to remove air bubbles trapped on its surface. Sufficient wetting of the target's surface can be achieved by its being wet sanded while it is submerged or by a rubber blade being repeatedly swept across its surface.

The weighting function $W(z; c_w)$ is fundamental to the characterization and calibration of backscattering sensors. In theory $W(z; c_w)$ could be calculated from first principles, but this would be extremely cumbersome because accurate analytic expressions are required for the cross-sectional profile of the beam and detector FOV. A better and almost certainly more accurate way to determine $W(z; c_w)$ is to measure it in some fashion. This can essentially be done through the measurement of $\Delta\Phi_\rho(z)$. Dividing Eq. (8) by $\cos\theta_s \cos\theta_d \exp[-c_w(r_s + r_d)]/r_d^2$ gives

$$\Delta\Phi_\rho(z)\{r_d^2 \exp[c_w(r_s + r_d)]/\cos\theta_s \cos\theta_d\} = k[\Delta A^2(z)/A(z)] \equiv kG(z), \quad (13)$$

where $k \equiv \Phi_0 g_\rho(\rho/\pi)$ is a constant and

$$G(z) \equiv \Delta A^2(z)/A(z), \quad (14)$$

which is strictly a function of the optical geometry of the sensor. Like $\cos\theta_s \cos\theta_d$, the factor $\exp[-c_w(r_s + r_d)]/r_d^2$ can easily be calculated based on the geometry in Fig. 5. The only empirical parameter is $c_w$ of the water in which $\Delta\Phi_\rho(z)$ is measured. This attenuation coefficient can be measured with a transmissometer or estimated by being assumed to be the value for pure water. The constant $k$ does not need to be known, because only the relative shape of $W(z; c_w)$ is needed. For example, the computation of $\sigma(c, c_w)$ given by Eq. (12) involves the ratio of $W(z; c_w)$ and $W(z; c)$, thus canceling $k$. Once $G(z)$ is computed from the formula on the left-hand side of Eq. (13), $W(z; c)$ can then be computed for any value of $c$ by way of Eq. (6). In other words, the measured sensor-response function $\Delta\Phi_\rho(z)$ to a Lambertian target provides all the information necessary to compute the weighting function $W(z; c)$ accurately, which is the key quantity for calibrating the backscattering sensor to provide a measurement of $\beta(\psi^*)$.

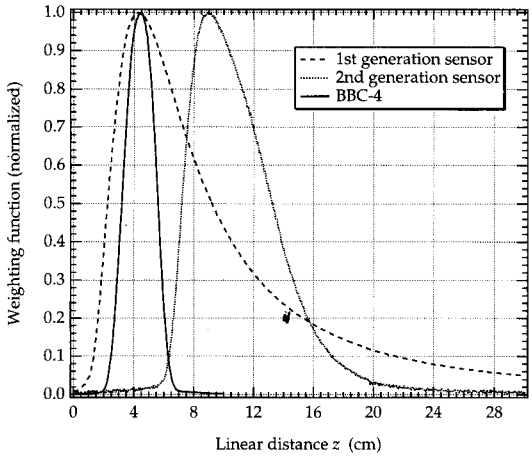


Fig. 6. Weighting functions of three backscattering sensors with different optical geometries. The more narrow the weighting function, the more collimated the optics of the sensor.

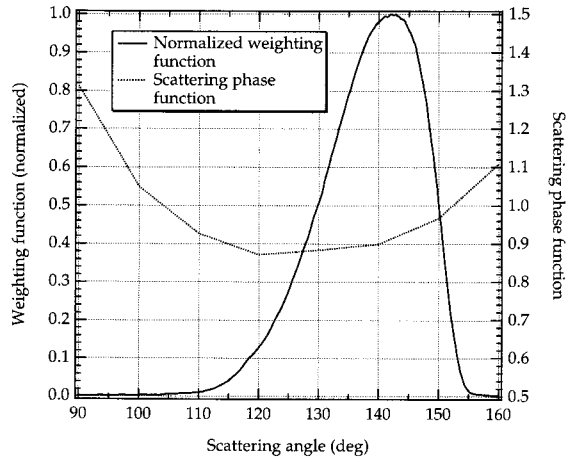


Fig. 7. $W(z; c)$ for the BBC-4 and Petzold average phase function plotted as a function of the scattering angle.

## 4. Analysis of Sensor Response and Calibration

### A. Sensor Analysis

We measured the in-water response of the backscattering sensors to a Lambertian target by using a motor-drive system that moves the target in a continuous fashion and digitally records its distance, simultaneously with the backscattering measurement, with an optical encoder. The tank water was filtered with a series of filters from 2- to 0.2-μm pore diameter. From the measured response function $\Delta\Phi_p(z)$ expressed by Eq. (8), the corresponding weighting function $W(z; c_w)$ as given by Eq. (6) was computed by the method described above.

Examples of $W(z; c_w)$ for all three major generations of backscattering sensors are shown in Fig. 6. The curves in this figure illustrate the evolution in the optical design of the backscattering sensors. For example, the first-generation sensor uses no collimating optics and thus has the broad weighting function shown in the figure. The second-generation sensor, which incorporates crude collimating optics, has a more narrow weighting function. Finally, the third-generation sensors, the BB-4, BBC-4, and HydroScat-6, which are designed with more highly collimating optics, yield the most narrow weighting function.

Recall Eq. (7), which shows that the detected scattered light is given by the integral of $\beta(\psi)$ weighted by $W(z; c)$. A perfect sensor with infinitesimal divergence angles would yield a delta function for $W(z; c)$, in which case $\beta(\psi)$ would be picked out at a discrete scattering angle given by the complement of the crossing angle of the (perfect) beam and receiver FOV. All real sensors must yield a $W(z; c)$ with a finite width, although the higher the collimation of the sensor optics, the smaller the width of $W(z; c)$, as shown above. The value of $\beta(\psi)$ that results from the calibrated measurement depends on the shapes of both $W(z; c)$ and $\beta(\psi)$ over the limits of integration, as required by the integral mean-value theorem. Sensor-response weighting functions tend to resemble skewed bell curves, as shown in Fig. 6, whereas the shape of $\beta(\psi)$ in the backward hemisphere is generally a broad U shape with a minimum somewhere between 100° and 140°. It should be expected then that the value of $\beta(\psi)$ or $\beta(\psi^*)$ that is picked out will tend to be near $\psi^*(z = z_{peak})$, where $z_{peak}$ is the distance $z$ at which the peak of $W(z; c)$ occurs.

Figure 7 illustrates these comments with a BBC-4 weighting function and a scattering phase function created by averaging the VSF measurements reported by Petzold,[2] which is probably indicative of the shapes of most if not all real ocean water phase functions. The phase function shown in Fig. 7 was normalized by $b_b$, not $b$, so that its solid-angle integration from 90° to 180° is unity. Both $W(z; c)$ and $\beta(\psi)$ are plotted as functions of $\psi$ over the range $z$ from ~1 to 10 cm. (As shown in Fig. 6, there is no sensor response below 1 or above 10 cm.) Clearly, multiplication of these two functions yields a curve that still closely resembles $W(z; c)$, so that the value of $\psi^*$ is determined almost entirely by $W(z; c)$. Figure 8 shows $\beta[\psi(z)]W[\psi(z); c]$, which appears almost exactly like $W(z; c)$ in Fig. 7. It is therefore an excellent approximation to assume that $\psi^*$ is given by $\psi^* = \psi(z^*)$, where

$$z^* \equiv \int_0^\infty zW(z; c)\mathrm{d}z \Big/ \int_0^\infty W(z; c)\mathrm{d}z \qquad (15)$$

is defined as the centroid of $W(z; c)$. If $W(z; c)$ is a symmetric function (such as a Gaussian), then $z^* = z_{peak}$. For the BBC-4 weighting function, $z^* = 4.21$ cm and $z_{peak} = 4.30$ cm. These correspond to scattering angles $\psi(z^*) = 141.2°$ and $\psi(z_{peak}) = 142.0°$. Numerically computing $\psi^*$ by finding that value of $\psi$ for which

$$\beta(\psi^*) = \int_0^\infty \beta[\psi(z)]W(z; c)\mathrm{d}z \Big/ \int_0^\infty W(z; c)\mathrm{d}z \qquad (16)$$

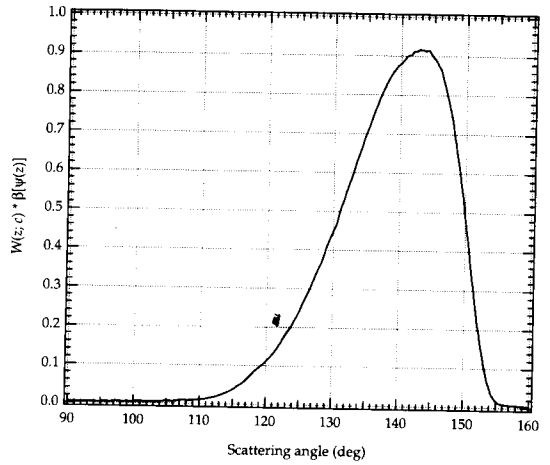


Fig. 8. $W[\psi(z); c_w]\beta[\psi(z)]$ as computed from the two curves in Fig. 7.

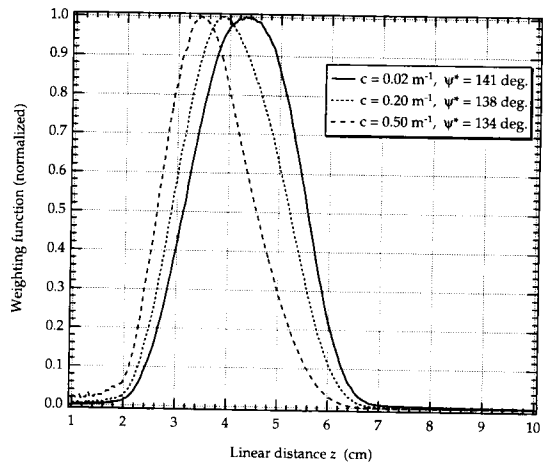


Fig. 9. $W(z; c)$ for three values of $c$. An increase in $c$ by a factor of 25 changed $\psi^*$ by only 7°.

gave $\psi^* = 141.3°$ when the Petzold average phase function was used. This value differs insignificantly from $\psi(z^*)$, demonstrating that Eq. (15), which is independent of $\beta(\psi)$, is an excellent way of computing $\psi^*$. It is recommended that $\psi^*$ be computed in this manner for all backscattering sensors and reported along with their backscattering measurements.

There remains the question of the dependence of $W(z; c)$ on the parameter $c$, which could in turn affect $z^*$ or $\psi^*$, since they are implicit functions of $c$ by virtue of Eqs. (15) and (16), respectively. $W(z; c)$, given by Eq. (6), can be expressed in the form

$$W(z; c) \equiv \exp[-c(r_s + r_d)]\left[\frac{G(z)\cos\theta_d}{r_d^2\cos\theta_s}\right],$$

where $G(z)$ is given by Eq. (14). The dependence of $W(z; c)$ on $c$ is therefore seen to be a function of only the factor $\exp(-cr) = \exp(-\tau)$, where $r \equiv r_s + r_d$ and $\tau \equiv c_r$. For the BBC-4, $r$ ranges from ~4 to 15 cm in the nonzero region of $W(z; c)$. If $c$ is of the order of, for example, 0.1 $m^{-1}$, $\tau$ ranges from 0.004 to 0.015, and $\exp(-\tau)$ changes in an approximate linear fashion from ~1.00 to 0.98. If $c$ is of the order of 1 $m^{-1}$, $\tau$ ranges from 0.04 to 0.15, and $\exp(-\tau)$ again changes in a linear fashion from 0.96 to 0.86. So $W(z; c)$ is not expected to be a strong function of $c$ for the BBC-4 optical geometry.

Figure 9 shows $W(z; c)$ for three different values of $c$. We normalized the three $W(z; c)$'s to unity to better illustrate the effect on the shapes of the curves and their centroid values, which is relevant to $\psi^*$. Although all three curves are approximately the same shape, there is a small but noticeable shift along the $z$ axis, which corresponds to a shift in $\psi^*$. The shift in $\psi^*$ is not large: A change in $c$ by a factor of 25 from 0.02 to 0.50 $m^{-1}$ changed $\psi^*$ by only 7°, from 141° to 134°. Nonetheless, this effect should be kept in mind, especially for measurements in coastal waters where drastic spatial variability in optical properties is often found. Moreover, this effect can be much greater for backscattering sensors with longer path lengths or wider optical geometries. This effect is probably most important for general-angle scattering meters that are designed to characterize the shape of the VSF.

One can understand the change in $\psi^*$ caused by a change in $c$ by referring to the optical geometry in Fig. 4. The total scattering volume is given by the intersection of the beam and detector FOV. However, the response of the sensor to each infinitesimal volume $dV$ within the total scattering volume is weighted by $W(z; c)$. In air, where there is no attenuation of light, the maximum response is at the distance $z_{peak}$ where $dV$ is a maximum, since $W(z; c)$ is now a function only of the geometry. In water the exponential attenuation of light with distance shifts the maximum response closer to the sensor faceplate. As the attenuation increases, $z_{peak}$ decreases.

One can compute the spectral correction factor $\sigma(c, c_w)$ given by Eq. (12), for any backscattering sensor by using the procedure described above for computing $W(z; c)$. The $W(z; c_w)$ from the filtered water calibration needs to be computed only once and then integrated. $W(z; c)$ can be computed repeatedly for a range of $c$'s and integrated. Taking the ratio of $\int W(z; c_w)dz$ and $\int W(z; c)dz$ for each value of $c$ yields a curve for $\sigma(c, c_w)$. Figure 10 gives the result for the 440-nm channel of the BBC-4. The initial $c$ value on the horizontal axis is $c_w = 0.02$ $m^{-1}$, which was measured with the BBC-4 transmissometer. This point corresponds to $\sigma(c, c_w) = \sigma(c_w, c_w) = 1$. Values below this were not computed because ocean water in which backscattering is measured should not be clearer than filtered laboratory water.

As expected from the foregoing discussion, $\sigma(c, c_w)$ is a small correction factor for relatively low values of $c$. Even a value of $c = 1$ $m^{-1}$ requires only an ~10% correction in $\beta(\psi^*)$. But a value of, say, $c = 4$ $m^{-1}$ requires almost a 50% correction in $\beta(\psi^*)$, which is significant. Such high values of $c$(440 nm) are often found in coastal and productive ocean waters. Moreover, in these regions vertical variability can be extreme, giving large changes in $c$ as well as $\beta(\psi^*)$, in

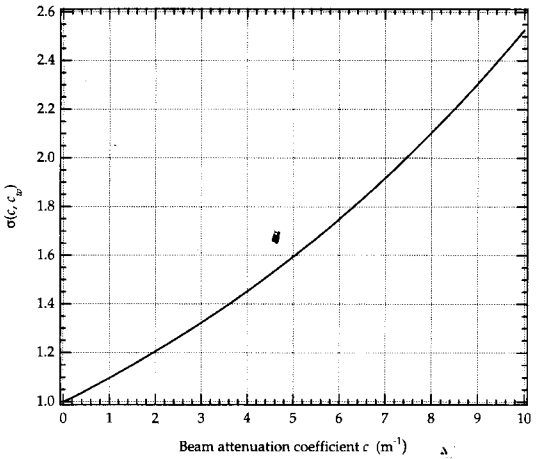


Fig. 10. Attenuation correction factor $\sigma(c, c_w)$ computed for the 440-nm channel of the BBC-4. The attenuation coefficient of the filtered water, $c_w = 0.02\ m^{-1}$ at 440 nm, was measured with the BBC-4 transmissometer.

a single profile. Although $\sigma(c, c_w)$ is a significant correction factor for high values of $c$, $\sigma(c, c_w)$ itself is a relatively weak function of $c$ at least for the optical geometry of the BBC-4 and is therefore insensitive to changes or errors in the measurement of $c$. It is important to appreciate this point. For example, a change in $c$ from 0.02 to 1 $m^{-1}$, which is a change by a factor of 50, results in only an ~10% change in $\sigma(c, c_w)$. In other words, inaccuracies in the measurement or estimation of $c$ used for computing $\sigma(c, c_w)$ generally have only a small effect on the accuracy of $\beta(\psi^*)$.

### B. Estimating the Backward-Scattering Coefficient

In principle, the backward-scattering coefficient $b_b$ can be determined by measuring $\beta(\psi)$ over the range 90–180° and then calculating its solid-angle integral over the backward hemisphere [see Eq. (3)]. For the routine measurement of $b_b$ in the ocean this is clearly impractical. A much simpler method is to measure $\beta$ at a single angle and then multiply it by a scaling factor to obtain $b_b$. Such an approach was actually first investigated in the search to develop a simple means of measuring the total scattering coefficient $b$. It is always true that at least one angle, denoted $\psi^*$, can be found such that $b_b = 2\pi\beta(\psi^*)$, which is justified by the integral mean value theorem,

$$\begin{aligned} b_b &= 2\pi\int_{\pi/2}^{\pi} \beta(\psi)\sin\psi d\psi \\ &= 2\pi\beta(\psi^*)\int_{\pi/2}^{\pi} \sin\psi d\psi \\ &= 2\pi\beta(\psi^*). \end{aligned} \tag{17}$$

Note that the angle $\psi^*$ depends only on the shape of the function $\beta(\psi)$ in the range 90–180°.

A properly calibrated fixed-angle backscattering sensor measures $\beta(\psi)$ at a single nominal angle that in general is not $\psi^*$ no matter how the sensor is designed. It is useful then to define the ratio

$$\chi \equiv \beta(\psi^*)/\beta(\psi_\chi), \tag{18}$$

where $\psi_\chi$ is the nominal scattering angle at which $\beta$ is measured by the backscattering sensor. Therefore

$$b_b = 2\pi\chi\beta(\psi_\chi). \tag{19}$$

It remains then to investigate, for a given value of $\psi_\chi$ that is fixed by the design of the sensor, the mean value and standard deviation of $\chi$ for the range of functions $\beta(\psi)$ expected to be found for oceanic waters.

Oishi[4] published an analysis on estimating $b_b$ from a single measurement of $\beta(\psi)$ in the backward hemisphere. His study focused mainly on Mie scattering functions for a polydisperse system of particles assumed to obey a Junge or hyperbolic size distribution, although he also included some empirical VSF data published by others. Oishi's conclusion was that $\beta(120°)$ gave the highest correlation to a linear expression for estimating $b_b$. Expressed another way, Oishi found that $\chi$ had the smallest standard deviation for $\psi_\chi = 120°$. At this angle he reports $\chi = 1.14$. A careful analysis of his results, however, also reveals that there is no statistically significant difference in using $\beta(120°)$, $\beta(130°)$, or $\beta(140°)$ in terms of the likely errors that result in the final estimation of $b_b$ using Eq. (19). Indeed, Oishi reports that the regression for $\beta(140°)$ gave a maximum predicted error that was less than that for $\beta(120°)$. Considering all of the uncertainties in his analysis, such as calculations using Mie theory and the meager empirical data set that was available, it might seem that the wiser choice is the angle that gives the lowest maximum prediction error. For 140° Oishi reports $\chi = 1.08$.

An analysis of one of the most well-documented empirical data sets of the VSF, namely, that of Petzold,[2] sheds further light on this issue. Petzold's ocean measurements fall into three categories: (1) clear ocean water measured in Tongue-of-the-Ocean, Bahamas, (2) coastal water measured off the coast of southern California, and (3) turbid water measured in the San Diego harbor. His results are summarized in Fig. 11 for the range 90°–180°, although $\beta(180°)$ was not actually measured and is an extrapolation by Petzold (which is not relevant to this discussion since these values are multiplied by $\sin\pi = 0$ in the integral for computing $b_b$). Each curve represents an average of all the data reported by Petzold for its particular category. The VSF's are normalized by the factor $2\pi/b_b$ for better comparison. Note that this phase function normalization is inversely related to $\chi$, that is, $2\pi\beta(\psi)/b_b = 1/\chi$.

It is immediately apparent from the three curves in Fig. 11 that $\psi_\chi \cong 120°$ yields the least variability in $\chi$, which was essentially Oishi's conclusion. Clearly, however, the turbid or harbor water average VSF is a statistical outlier. Whether this is due to measurement errors or is a real phenomenon remains an open

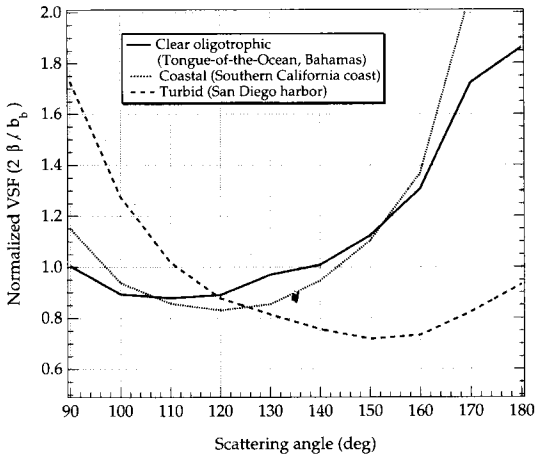


Fig. 11. VSF measurements by Petzold[2] normalized by the factor $2\pi/b_b$. Each curve is an average of all the data reported by Petzold for that water type.

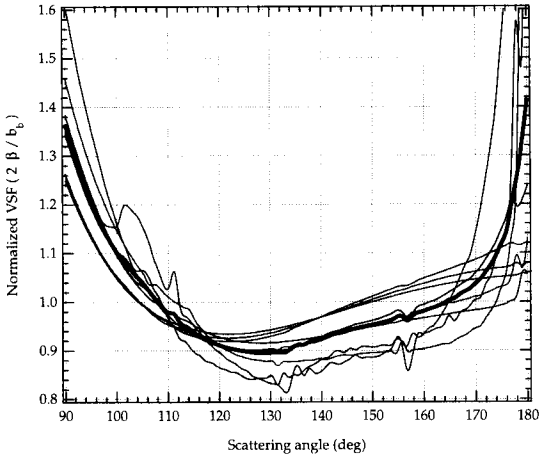


Fig. 12. Computations of the VSF using Mie theory and assuming a Junge or hyperbolic particle-size distribution. Curves are normalized by the factor $2\pi\beta(\psi)/b_b = 1/\chi$. The thick solid curve is the average of all the VSF's.

question. But the fact is that, as far as the empirical evidence is concerned, there is little variability in these curves (excluding the turbid harbor water) and thus in $\chi$ over the middle range of scattering angles for the vast majority of oceanic waters.

It is nonetheless unsatisfying to rest conclusions solely on the basis of scant empirical VSF data that is incomplete, unverified, and has not been systematically investigated in nearly 25 years. The only other recourse at this time is the theory of Mie.[16,17] Similar to the investigation conducted by Oishi, we thus performed a series of calculations of the VSF using the Mie theory and the computer algorithms published in Bohren and Huffman[18] with some modifications. These calculations were performed for a realistic range of particle refractive indices and particle-size distributions. The real part of the particle relative refractive index was varied from 1.05 to 1.15. There was no meaningful effect owing to a nonzero imaginary refractive index within expected values. The particle-size distribution density function was taken to be a Junge (hyperbolic) distribution, and the exponent or slope on a logarithmic scale of the distribution was varied from 3.5 to 4.5, which covers the range of values found in the literature. Moreover, we performed these calculations over a range of visible wavelengths from 410 to 675 nm.

The results of these calculations are summarized in the graph shown in Fig. 12. The VSF's are normalized by the factor $\tilde{\beta}(\psi) \equiv 2\pi\beta(\psi)/b_b$; note that $\tilde{\beta}(\psi) = 1/\chi$. Nine phase functions are shown that represent the largest spread of all the calculated $\tilde{\beta}(\psi)$'s. The thick solid curve is the average of all the phase functions. It was found that the slope of the particle-size distribution had the strongest effect on the variability of $\tilde{\beta}(\psi)$ and therefore $\chi$. The phase function was least sensitive to changes in wavelength across the visible spectrum. Thus for all practical purposes $\chi$ can be considered independent of wavelength. Varying the particle refractive index had some affect on the variability of $\tilde{\beta}(\psi)$, but it was significant only at angles greater than 160°. The standard deviation in taking the average of all of the phase functions was statistically a minimum over the angular range 112°–119°. The percent deviation (i.e., the standard deviation divided by the average and multiplied by 100) in this angular range was ~5%. The largest deviations were found at the end angles, namely 90° and 180°, which is also clearly apparent in Fig. 12. At 140°, which is the centroid response angle of the BBC-4 sensor, the percent deviation in $\chi$ was 9% and the average was $\chi = 1.08$, which is in agreement with the value reported by Oishi.

## 5. Summary and Conclusions

A rigorous analysis of fixed-angle backscattering sensors has shown that the sensor response to volume scattering can be expressed as a weighted integral of the VSF [Eq. (7)] over the sensor's angular response. The weighting or sensor-response function $W(z; c)$ given by Eq. (6) was shown to be a function of both the geometry of the sensor, which is fixed, and the beam attenuation coefficient $c$ of the water, which is variable. However, the derivation of $W(z; c)$ showed that it could be separated analytically into two factors, one solely a function of the sensor optical geometry, $G(z)$ given by Eq. (14), and the other a simple exponential function of $c$.

The weighting function is fundamental to calibrating backscattering sensors and interpreting their measurements properly. A procedure was given for accurately determining a sensor's weighting function. This procedure involves first measuring the in-water response of the sensor to a Lambertian target as a function of distance $z$. Dividing this measured response function $\Delta\Phi_p(z)$ given by Eq. (8) by $\cos\theta_s \cos\theta_d$ then yields $W(z; c_w)$ to within a multiplicative constant that does not need to be known. $G(z)$ can also be calculated from $\Delta\Phi_p(z)$, as shown by Eq.

(13). Once $G(z)$ is known, $W(z; c)$ can be calculated for any value of $c$.

When $W(z; c)$ for a particular backscattering sensor is known, the sensor can be calibrated accurately to yield measurements of $\beta(\psi^*)$ in absolute units, in which $\psi^*$ was shown to be a close approximation to the centroid angle of $W(z; c)$. Because $W(z; c)$ depends on $c$, $\psi^*$ does as well, although it was shown to be only a weak function of $c$. In the worse case $\psi^*$ changed by $\sim 10°$ when $c$ changed by a factor of 25.

We derived a correction factor $\sigma(c, c_w)$ given by Eq. (12) that corrects the backscattering measurement for the light attenuation by the water. $\sigma(c, c_w)$, like $\psi^*$, was also shown to be a weak function of $c$. However, for coastal and productive oceanic waters, where $c$ can often be large and also highly variable, neglecting the $\sigma(c, c_w)$ correction can result in significant errors in backscattering measurements.

An analysis of a recently developed four-wavelength backscattering sensor, the BBC-4, showed that $\psi^* = 141°$ at $c_w = 0.02\ \mathrm{m}^{-1}$ (440 nm). For all backscattering sensors $\psi^*$ decreases with increasing $c$ and asymptotes to some minimum value that depends on the sensor's optical geometry. For the BBC-4 this minimum value was found to be $\psi^* = 134$ at $c(440\ \mathrm{nm}) = 0.5\ \mathrm{m}^{-1}$.

We investigated the conjecture that the backward-scattering coefficient $b_b$ can be estimated with a measurement of the VSF at a single angle in the backward hemisphere. VSF measurements by Petzold[2] show little variability in $\tilde{\beta}(\psi) = 1/\chi$ from clear blue oceanic waters to coastal waters. The only significant change in $\tilde{\beta}(\psi)$ was for the highly turbid San Diego harbor water. Mie theory calculations of the VSF reveal that the slope of the particle-size distribution has the strongest affect on the variability in $\tilde{\beta}(\psi)$. Nonetheless, for a wide range of calculations the percent deviation in $\chi$ was between 5% and 10% of the average value over the middle range of scattering angles, which is the response range of our fixed-angle backscattering sensors. For a centroid response angle of 140° the statistically best equation for converting the calibrated measurement of $\beta(\psi^*)$ to $b_b$ is $b_b = 2\pi \times 1.08\beta(\psi^*)$. The standard percent error in this estimate was calculated to be $\sim 9\%$. Thus the backward-scattering coefficient can be fairly accurately computed from measurements with fixed-angle backscattering sensors, assuming that the sensors are properly calibrated and that their response functions cover the middle range of backscattering angles.

Several people at SRI International contributed to the initial development of optical backscattering sensors in one way or another. Special acknowledgment and sincere thanks go to Richard Honey and Jeff Voss. This study was supported by the Environmental Optics Program at the Office of Naval Research.

## References

1. W. S. Pegau, J. S. Cleveland, W. Doss, C. D. Kennedy, R. A. Maffione, J. L. Mueller, R. Stone, C. C. Trees, A. D. Weidemann, W. H. Wells, and J. R. V. Zaneveld, "A comparison of methods for the measurement of the absorption coefficient in natural waters," J. Geophys. Res. **100,** 13,201–13,220 (1995).
2. T. J. Petzold, "Volume scattering functions for selected ocean waters," Scripps Institution of Oceanography Rep. No. 72-78 (Scripps Institution of Oceanography, La Jolla, Calif., 1972).
3. G. Kullenberg, "Observed and computed scattering functions," in *Optical Aspects of Oceanography*, N. G. Jerlov and E. S. Nielsen, eds. (Academic, New York, 1974), pp. 25–49.
4. T. Oishi, "Significant relationship between the backward scattering coefficient of sea water and the scatterance at 120°," Appl. Opt. **29,** 4658–4665 (1990).
5. N. Højerslev, "A history of early optical oceanographic instrument design in Scandinavia," in *Ocean Optics*, R. W. Spinrad, K. L. Carder, and M. J. Perry, eds. (Oxford University Press, New York, 1994), Chap. 7, pp. 118–147.
6. H. Pettersson, "A transparency-meter for sea-water," Medd. Oceanogr. Inst. Gothenburg, Ser. B **4,** (1934).
7. J. E. Tyler and W. H. Richardson, "Nephelometer for the measurement of volume scattering function *in situ*," J. Opt. Soc. Am. **48,** 354–357 (1958).
8. C. A. Moore, R. Honey, D. Hancock, S. Damron, and R. Hilbers, "Development and use of computerized optical sea-truth instrumentation for LIDEX-82," SRI International Project 3878 Final Rep. (SRI International, Menlo Park, Calif., 1984).
9. R. A. Maffione, D. R. Dana, and R. C. Honey, "Instrument for underwater measurement of optical backscatter," in *Underwater Imaging, Photography, and Visibility*, R. W. Spinrad, ed., Proc. SPIE **1537,** 173–184 (1991).
10. J. H. Smart, A. B. Fraser, and M. J. Jose, "Variability in optical properties across the Gulf of Alaska," Proc. Oceans (*Honolulu, Haw.*) **91,** 657–666 (1991).
11. R. A. Maffione, D. R. Dana, and J. M. Voss, "Spectral dependence of optical backscattering in the ocean," presented at the OSA Annual Meeting, Portland, Oregon, 1995 (Optical Society of America, Washington, D.C.).
12. R. A. Maffione, D. R. Dana, J. M. Voss, and G. S. Frysinger, "Instrumented remotely operated vehicle for measuring inherent and apparent optical properties of the ocean," in *Underwater Light Measurements*, H. C. Eilertsen, ed., Proc. SPIE **2048,** 124–137.
13. H. R. Gordon, O. B. Brown, and M. M. Jacobs, "Computed relations between the inherent and apparent optical properties of a flat homogeneous ocean," Appl. Opt. **14,** 417–427 (1975).
14. A. Morel and L. Prieur, "Analysis of variations in ocean color," Limnol. Oceanogr. **22,** 709–722 (1977).
15. N. G. Jerlov, *Marine Optics*, 2nd ed. (Elsevier, New York, 1976), p. 231.
16. G. Mie, "Beiträge zur optik trüber median, speziell kolloidaler metallösungen," Ann. Phys. **25,** 377–442 (1908).
17. H. C. van de Hulst, *Light Scattering by Small Particles* (Wiley, New York, 1957), p. 470.
18. C. F. Bohren and D. R. Huffman, *Absorption and Scattering of Light by Small Particles* (Wiley, New York, 1983), p. 530.